8 Longitudinal Phase Space Manipulation

In this chapter we describe various techniques used to control the longitudinal properties of particle beams. We concentrate on the manipulation of the second moments of the longitudinal distribution; that is, on the bunch length and energy spread. As will be shown, the bunch length can be varied using accelerating cavities to compress, coalesce, split, and lengthen stored bunches. The energy spread of the beam can also be adjusted (usually to be a minimum) by proper phasing of the rf, by invoking cancellations between the applied and beam-induced rf, and by more sophisticated techniques for the case of long bunch trains. A practical application of the use of rf systems to affect the beam's transverse emittance is presented lastly.

8.1 Bunch Length Compression

Bunch length compression using dedicated accelerating structures and beamlines is common to all linear collider designs [1, 2, 3] and FEL linac drivers [4, 5]. Compression is usually performed in two or more steps. First an rf section (for example an accelerating structure) is used to introduce a correlation between the particle energy and position within a bunch. In the second step the beam passes through a transport line with nonzero dispersion (i.e., bends) where the actual compression occurs due to the energy dependence of the particle trajectory.

If the bunch is made to arrive near a zero crossing of the rf wave with the voltage decreasing from positive to negative values, the longitudinal phase space through the compressor evolves then as follows. Let (z_1, δ_1), (z_2, δ_2), and (z_3, δ_3) denote the longitudinal position z and relative energy δ at the entrance of the compressor, downstream of the compressor rf structure, and at the end of the compressor, respectively. A particle within the bunch is transported through the compressor cavity as

$$\begin{aligned} z_2 &= z_1 \\ \delta_2 &= \delta_1 - \frac{eV_{\mathrm{rf}}}{E} \sin\phi \,, \end{aligned} \tag{8.1}$$

where e is the particle charge, V_{rf} is the compressor voltage, E is the beam energy, and ϕ is the relative phase of the particle with respect to the zero cross-

M. G. Minty et al., *Measurement and Control of Charged Particle Beams,*
https://doi.org/10.1007/978-3-662-08581-3_8

ing of the compressor voltage. A particle arriving earlier ($\phi < 0$), will acquire a higher energy ($\delta_2 > \delta_1$). The phase ϕ can also be written as $\phi \equiv \phi_1 - \phi_c$, where ϕ_1 is the phase of the particle and ϕ_c the phase of the compressor rf voltage, both with respect to a common reference.

For simplicity, in this section we consider an ultrarelativistic particle, travelling at the speed of light, and thus, we do not distinguish between relative momentum deviation and relative energy deviation. Under this assumption, after passing through the dispersive downstream arc, the longitudinal position of a particle is

$$\begin{aligned} z_3 &= z_2 + R_{56}\delta_2 \\ \delta_3 &= \delta_2 \ . \end{aligned} \tag{8.2}$$

A particle, which after the compressor cavity has a higher energy than nominal ($\delta_2 > 0$), will be slowed down, i.e., $z_3 < z_2$, provided R_{56} is less than zero, as is the case for a regular arc. For a non-relativistic particle, (8.2) must be modified to include an additional factor $\beta = v/c$ (velocity divided by the speed of light) and a term representing the effect of the change in velocity.

Combining (8.1) and (8.2), the particle's longitudinal position and energy at the exit of the compressor are given in terms of its initial values by

$$\begin{aligned} z_3 &= z_1 + R_{56}\left(\delta_1 - \frac{eV_{\rm rf}}{E}\sin\phi\right) \\ \delta_3 &= \delta_1 - \frac{eV_{\rm rf}}{E}\sin\phi \ . \end{aligned} \tag{8.3}$$

The phase ϕ is related to the initial longitudinal position via $\phi = -\omega_{\rm rf} z_1/c$ (a positive z indicates a position ahead of the bunch center). If the phases are small compared with π, we may linearly expand the sine function, and (8.3) can be approximated by

$$\begin{aligned} z_3 &\approx \left(1 + R_{56}\frac{e\omega_{\rm rf}V_{\rm rf}}{cE}\right)\ z_1 + R_{56}\delta_1 \\ \delta_3 &\approx \delta_1 - \frac{eV_{\rm rf}\omega_{\rm rf}}{cE}\ z_1 \ . \end{aligned} \tag{8.4}$$

Then the final bunch length is

$$\sigma_{z,f} = \langle {z_3}^2 \rangle^{1/2} \approx \sqrt{\left(1 + R_{56}\frac{eV_{\rm rf}\omega_{\rm rf}}{Ec}\right)^2 \sigma_{z,0}^2 + R_{56}^2\sigma_{\delta,0}^2} \ , \tag{8.5}$$

where σ_{z0} is the initial bunch length and $\sigma_{\delta,0}$ is the initial beam energy spread. In the approximation it has been assumed that the incoming beam distribution has no energy-position correlation ($\langle \delta_1 z_1 \rangle = 0$). If the rf voltage is adjusted to give

$$-R_{56}\frac{eV_{\rm rf}\omega_{\rm rf}}{Ec} = 1 \ , \tag{8.6}$$

then the final bunch length is minimum, equal to $R_{56}\sigma_{\delta,0}$ and is independent of the initial bunch length, σ_{z0}. This is called the condition for full compression. If the voltage is smaller, one operates with undercompression, and for higher rf voltage one has overcompression.

According to (8.5), a larger compressor voltage and a smaller value of R_{56} may provide shorter bunches. However, as can easily be inferred from (8.3), for large rf voltages the final energy spread increases roughly in proportion to the rf voltage. Given a limited momentum acceptance in the downstream system, a compromise has to be made, which introduces a lower limit on R_{56}.

Phase errors and phase fluctuations may be critical in a compressor, particularly if the compression takes place upstream of a linear accelerator with strict tolerances on the injection phase[1]. For the (single-stage) compressor scheme described above with $\phi = -\omega z/c$, the resulting beam phase ϕ_3 in terms of the initial beam phase ϕ_1 is

$$\begin{aligned}\phi_3 &= \phi_1 - R_{56}\frac{\omega}{c}\left[\delta_1 - \frac{eV_{\mathrm{rf}}}{E}\sin(\phi_1 - \phi_c)\right] \\ &\approx -R_{56}\frac{\omega}{c}\delta_1 + \left[1 + R_{56}\frac{\omega_{\mathrm{rf}}}{c}\frac{eV}{E}\right]\phi_1 - R_{56}\frac{\omega_{\mathrm{rf}}}{c}\frac{eV_{\mathrm{rf}}}{E}\phi_c\,, \end{aligned} \tag{8.7}$$

where ω_{rf} is the angular accelerating frequency of the structure. Assuming that the errors in the injected beam phase $\Delta\phi_i$ and the compressor phase $\Delta\phi_c$ are independent, and that the initial momentum deviations are independent of these phases ($\mathrm{d}\delta_1/\mathrm{d}\phi_1 = \mathrm{d}\delta_1/\mathrm{d}\phi_c = 0$) we find

$$\frac{\mathrm{d}\phi_3}{\mathrm{d}\phi_c} = \eta \quad \text{and} \quad \frac{\mathrm{d}\phi_3}{\mathrm{d}\phi_1} = 1 + \eta \ , \tag{8.8}$$

where we have defined $\eta \equiv (-R_{56}\frac{\omega_{\mathrm{rf}}}{c}\frac{eV}{E})$. Combining the two contributions of (8.7) in quadrature gives for the final phase error

$$(\Delta\phi_3)^2 = \eta^2(\Delta\phi_c)^2 + (1+\eta)^2(\Delta\phi_1)^2 \ . \tag{8.9}$$

In particular, for $\eta = -1$ (full compression) the final phase is independent of the initial phase error $\Delta\phi_1$.

An example of a bunch compressor designed for the Next Linear Collider [6] is shown in Fig. 8.1. This design comprises a two-fold compression scheme. The principle of the first bunch compressor (BC1) is as described above, but with an energy-dependent path length generated by a wiggler magnet with $R_{56} < 0$. At higher energy, the second bunch compression (BC2) is performed, which consists of an arc, a second rf section, and a magnetic chicane. In BC2 a net 360° phase space rotation is used to minimize the sensitivity to incoming energy errors, which might arise either from phase errors at the entrance to BC1 of from beam loading in the linac located between BC1 and BC2.

[1] at the SLC, the phase stability at injection into the main linac required for imperceptible influence on the luminosity was $< 0.1°$, or < 1 ps, at the linac frequency of 2856 MHz

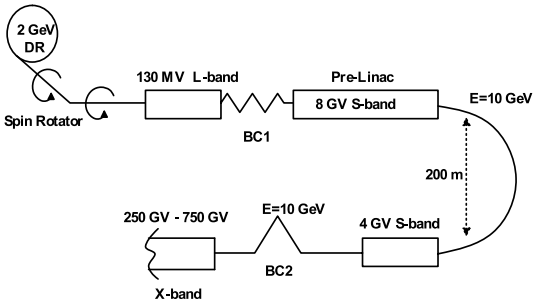

Fig. 8.1. Schematic of an NLC bunch compressor [6]

8.2 Bunch Length Precompression

Bunch precompression by means of rf systems is frequently used for reducing the bunch length (at the expense of an increased energy spread) for transferral of particle beams from one accelerator to a downstream accelerator operating at higher rf frequency. Bunch precompression has also been used to alleviate the consequences of current-dependent bunch lengthening (i.e., beam loss) in lepton accelerators.

For a relativistic beam ($\alpha_c - 1/\gamma^2 \approx \alpha_c$), the equation of motion for the bunch length, $\sigma_z = \sigma_\phi(c/w)$, is obtained as follows. Using a dot to denote a derivative with resepct to time, i.e.,

$$\dot{()} \equiv \frac{\mathrm{d}}{\mathrm{d}t}() \quad \text{and} \quad \ddot{()} \equiv \frac{\mathrm{d}^2}{\mathrm{d}t^2}() \ , \tag{8.10}$$

and the equalities

$$\begin{aligned} \langle \dot{\phi^2} \rangle &= 2\langle \phi\dot{\phi} \rangle \ , \\ \langle \dot{\phi\delta} \rangle &= \langle \phi\dot{\delta} + \dot{\phi}\delta \rangle \ , \\ \langle \dot{\delta^2} \rangle &= 2\langle \delta\dot{\delta} \rangle \ , \end{aligned} \tag{8.11}$$

one finds

$$\begin{aligned} \langle \ddot{\phi^2} \rangle &= \frac{\mathrm{d}}{\mathrm{d}t} 2\langle \phi\dot{\phi} \rangle = 2\alpha\omega\langle \dot{\phi\delta} \rangle \text{ using } \ (7.1) \\ &= -\frac{2\alpha e\dot{V}}{ET}\langle \phi^2 \rangle + 2(\alpha\omega)^2 \left[\frac{1}{\langle \phi^2 \rangle} \left(\epsilon^2 + \frac{\langle \dot{\phi^2} \rangle^2}{(2\alpha\omega)^2} \right) \right] \\ &= -\frac{2\alpha e\dot{V}}{ET}\langle \phi^2 \rangle + \frac{2(\alpha\omega)^2}{\langle \phi^2 \rangle}\epsilon^2 + \frac{1}{2}\frac{\langle \dot{\phi^2} \rangle^2}{\langle \phi^2 \rangle} \ , \end{aligned} \tag{8.12}$$

where we have used the definition of the longitudinal emittance ϵ

$$\epsilon^2 = \langle \phi^2 \rangle \langle \delta^2 \rangle - \langle \phi\delta \rangle^2 \ . \tag{8.13}$$

Using

$$\frac{\mathrm{d}^2}{\mathrm{d}t^2}\sigma_\phi^2 = 2(\sigma_\phi\ddot{\sigma}_\phi + \dot{\sigma}_\phi^2) \,, \tag{8.14}$$

the equation of motion for the bunch length (in phase units) is

$$\ddot{\sigma_\phi} = -\frac{\alpha_c e\dot{V}}{ET}\sigma_\phi + \frac{(\alpha_c\omega_{\mathrm{rf}})^2\epsilon^2}{{\sigma_\phi}^3} \,, \tag{8.15}$$

where $\dot{V}$ was given in (7.3). A similar analysis for the rms energy spread is likewise calculable. The results are summarized [7] as

$$\begin{aligned} \ddot{\sigma_\phi} - {\omega_s}^2\sigma_\phi &= (\alpha\omega_s)^2\frac{\epsilon^2}{{\sigma_\phi}^3} \,, \\ \ddot{\sigma_\delta} - {\omega_s}^2\sigma_\delta &= \frac{(e\dot{V})^2}{E\omega T}\frac{\epsilon^2}{{\sigma_\phi}^3} \,. \end{aligned} \tag{8.16}$$

Bunch rotations are used for better capture efficiency of the proton beam at HERA [8, 9]. There two schemes were tried to shorten the bunch at extraction from the upstream PETRA ring. Initially, the bunch rotation was made by introducing a 180° phase jump in the accelerating rf which places the beam distribution next to an unstable fixed point. The ensuing slow motion of particles along the separatrices translates into a mismatch. The phase was then restored to its original setting and the beam was extracted about a quarter of a synchrotron period later. Beam loading effects however caused bunch shape distortions during the phase jump [8].

Presently bunch precompression at HERA is achieved by amplitude modulating the rf system to induce a quadrupole mode oscillation. A similar scheme was used at the SLC damping ring primarily for reducing transmission losses in the downstream transport line [7]. Here bunch precompression was implemented in a two step process (see Ex. 8.2). The first step change in the requested cavity voltage resulted in a longitudinal phase space mismatch which elongated the bunch. The resulting beam phase oscillation was then eliminated while amplifying the bunch length oscillation by application of a second, appropriately timed, step change to the cavity voltage.

Figure 8.2 shows diagnostic measurements illustrating bunch precompression from the SLC. Plotted are the cavity voltage (measured using a diode detector), the bunch length (obtained from a peak current measurement, which is inversely proportional to the bunch length, using a single stripline of a position monitor), and the mean energy of the beam. The centroid energy was measured using a horizontal beam position monitor in a region of high dispersion in the damping ring. The peak-current signal at extraction was increased, corresponding to a shorter bunch.

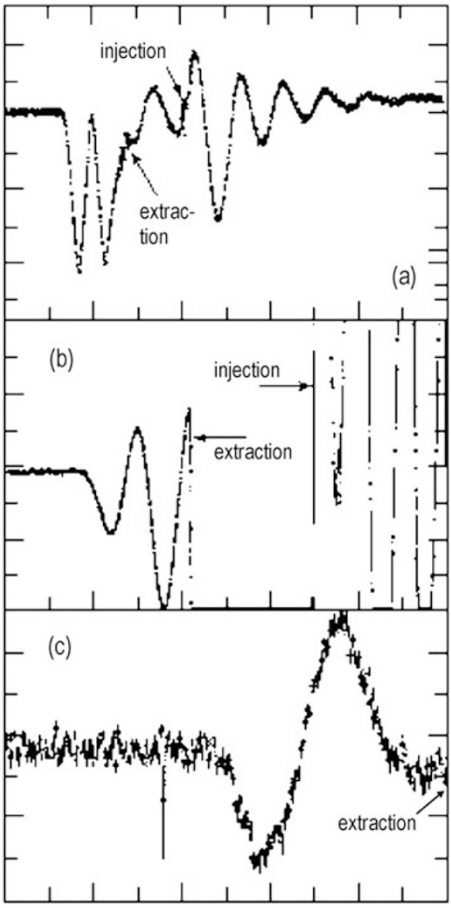

Fig. 8.2. Bunch precompression in the SLC damping rings: (**a**) measured cavity voltage [50 kV/dvsn, 10 μs/dvsn], (**b**) peak current [10%/dvsn, 5 μs/dvsn], and (**c**) centroid energy [50 μm or 0.77%/dvsn, 20 turns or 2.34 μs/dvsn]

8.3 Bunch Coalescing

Bunch coalescing, used primarily in hadron accelerators, consists of combining multiple bunches into a single bunch in order to achieve a high peak intensity. At Fermilab two types of coalescing are used [10]: standard coalescing for the low intensity antiprotons and 'snap' coalescing for high intensity proton beams.

Experimental data from the Fermilab Main Ring are shown in Fig. 8.3 which demonstrate the bunch coalescing concept. The different traces correspond to different times. Initially there were 11 bunches captured in 53 MHz rf buckets. The vector sum of the rf voltages was then adiabatically reduced, or 'paraphased' by shifting the relative phases between the accelerating cavities, which lengthens the bunch while preserving the longitudinal beam emittance.

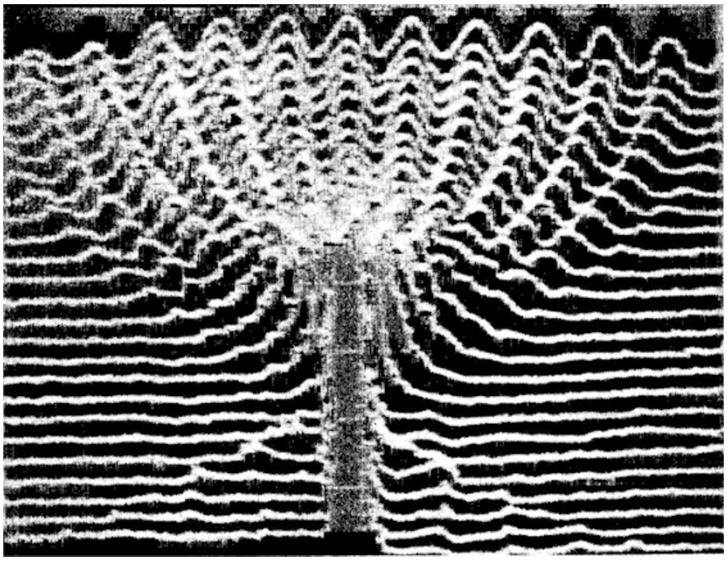

Fig. 8.3. Experimental data from the Fermilab main ring showing multiple bunches being coalesced into a single bunch. Successive traces are spaced by 6.8 ms intervals (Courtesy P. Martin, 1999)

The bunches were next subjected to a higher voltage 2.5 MHz rf system. The bunches rotate with the synchrotron frequency in this low frequency rf potential. In practice [11], a 5 MHz rf is also applied to help linearize the rotation. When the bunches were vertically aligned in the 2.5 MHz rf bucket, they are finally captured in a single 53 MHz rf bucket.

The *snap coalescing* scheme replaces the adiabatic voltage reduction from above with a phase space rotation. Here the coalescing procedure is initiated with a fast reduction of the primary rf amplitude. The beam is then longitudinally mismatched and shears in longitudinal phase space. After one quarter synchrotron oscillation the low frequency rf systems are turned on and the bunches are recaptured back into the primary rf bucket. Simulations [10] have shown that the capture efficiency of snap coalescing is about 10% less than with the adiabatic coalescing. However, at high currents, beam instabilities have been observed during adiabatic paraphasing of the 53 MHz rf systems. This is avoided with snap coalescing..

Two practical issues associated with bunch coalescing are the increased longitudinal emittance (minimized by adjusting the amplitude of the rf during initial bunch lengthening) and the production of satellite bunches (i.e., particles in neighboring rf buckets) which can arise during the recapturing process due to rf nonlinearities. The satellite bunches, which can cause detector backgrounds, may be eliminated using a longitudinal damper to discard the offending bunches [12]. Recently new 2.5 MHz cavities have been installed in the main ring allowing for a threefold increase in the vector voltage at this

lower frequency. The coalescing efficiencies were increased by 14% for the antiproton beam and 10% for the proton beam and the satellite bunches were eliminated using the new cavities [13].

8.4 Bunch Splitting

The LHC beam may consist of bunch trains of 72 bunches each containing about 10^{11} protons with a 25 ns bunch-to-bunch spacing. The original concept for producing these bunch trains in the proton synchrotron (PS) was to debunch 6 or 7 highly intense bunches and then to recapture the beam using a higher frequency rf system. A longitudinal microwave instability arose during the debunching and rebunching process [14] however and resulted in non-uniform beam distributions.

An alternate solution was adapted consisting of splitting of bunches using additional harmonic cavities in the injection chain for the Large Hadron Collider (LHC) [15]. To produce as many bunches as possible, the bunches are split in the upstream PS accelerator in a 2 step process. First, at low proton momentum (3.57 GeV/c) each of the 6 bunches from the booster ring is split into 3 as shown in the simulation results of Fig. 8.4. Then, after ramping to high momentum (26 GeV/c) the bunches are further split into 4, as shown in Fig. 8.5. On the left of these figures is shown the relative amplitude of each of the different harmonic rf systems as a function of time during the bunch splitting process.

Such bunch splitting has first been experimentally demonstrated [17] in the PS booster at CERN in application to neutrino experiments. Shown in Fig. 8.6 is the measured evolution of the longitudinal distribution using tomographic measurement techniques [18, 19] from the CERN PS [15, 19]. Plotted

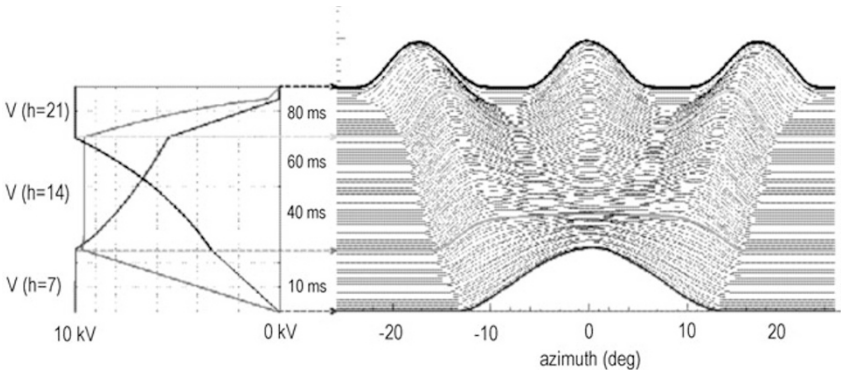

Fig. 8.4. Simulation of bunch triple splitting in the CERN PS at low energy (3.57 GeV/c) in preparation for injection into the LHC. Compare with the measurements shown in Fig. 8.7 (Courtesy R. Garoby, 1999)

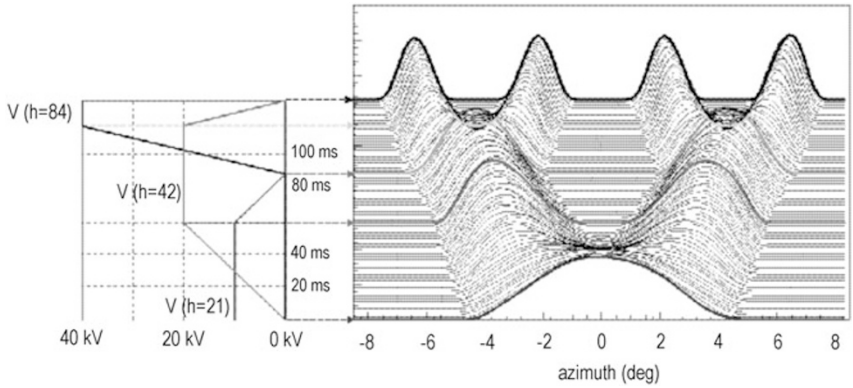

Fig. 8.5. Simulation of further bunch splitting in the CERN PS at high energy (26 GeV/c) in preparation for injection into the LHC. Compare with the measurements shown in Fig. 8.8 (Courtesy R. Garoby, 1999)

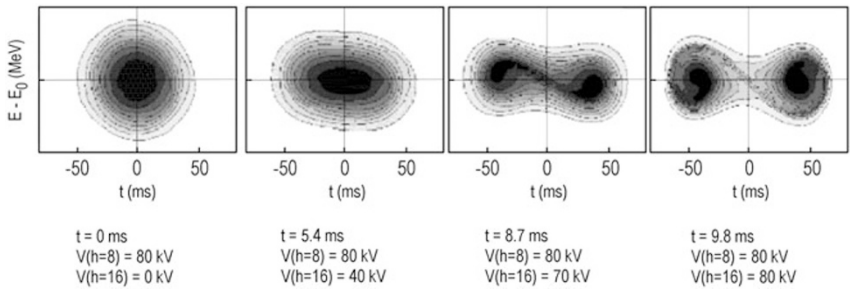

Fig. 8.6. Tomographically reconstructed phase space showing bunch splitting in the CERN PS booster ring after acceleration with 3×10^{12} protons (Courtesy R. Garoby, 1999)

is the phase space at the indicated times, and the corresponding amplitudes of the primary and harmonic cavity voltages are indicated below each picture.

After a series of hardware upgrades the feasibility of the bunch filling scheme required for the LHC has been demonstrated [14] in the CERN PS ring. First the triple-splitting scheme was verified experimentally [20], and then the newly installed harmonic cavities operating at 40 MHz ($h = 84$) and 80 MHz ($h = 168$) were used to accommodate also bunch quadruple-splitting and bunch rotation [16]–[21]. In the triple-splitting scheme, the 10 ferrite-loaded cavities of the PS were tuned before the splitting process as follows: 4 inactive, 2 at $h = 7$, 2 at $h = 14$, and 2 at $h = 21$. After splitting, as shown in Fig. 8.7, all cavities were tuned on $h = 21$ to allow full rf voltage for further acceleration.

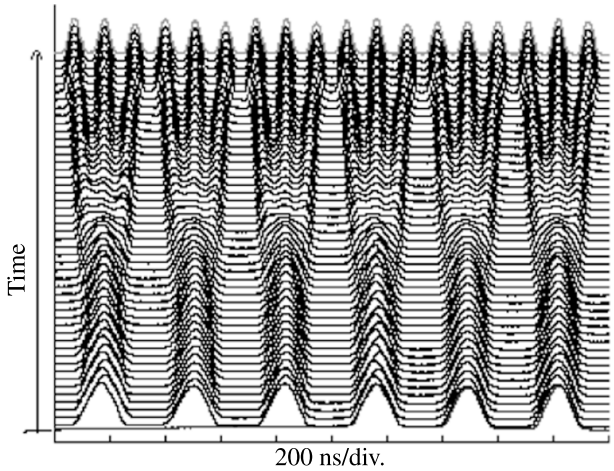

Fig. 8.7. Measured bunch triple-splitting at the CERN PS ($E = 1.4$ GeV, $I_p = 8 \times 10^{12}$, 400 revolutions per trace). Compare with Fig. 8.4 (Courtesy R. Garoby, 2001)

The quadruple splitting was achieved in two steps as shown in the measured results of Fig. 8.8. The bunches were then rotated in longitudinal phase space using the 40 and 80 MHz cavities to match into the acceptance of the downstream Super Protron Synchrotron (SPS) accelerator. This bunch splitting technique is used in routine operation of the CERN PS for the pro-

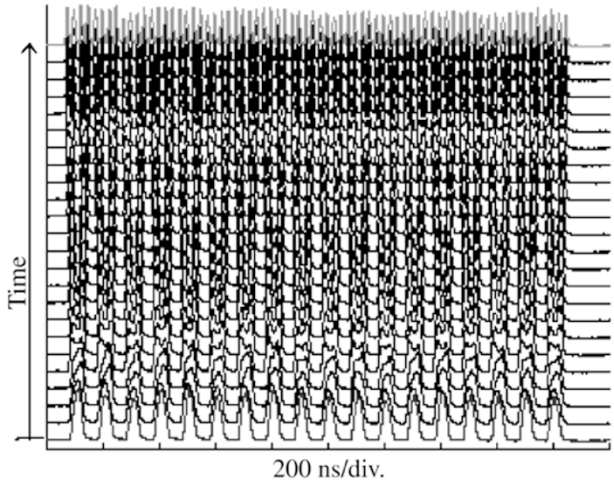

Fig. 8.8. Subsequent quadruple splitting at the CERN PS ($E = 25$ GeV, $I_p = 8 \times 10^{12}$, 1250 revolutions per trace). Compare with Fig. 8.5 (Courtesy R. Garoby, 2001)

duction of an LHC type beam which is sent to the SPS, where it is further accelerated up to the LHC injection energy of 450 GeV.

At the IUCF Cooler Ring, using a different technique proton bunches were observed to split by application of either a phase [22] or an amplitude [23, 24] modulation of the rf signal driving the accelerating cavities. An example is shown in Fig. 8.9. In this case, longitudinal modulation resulted from application of a sinusoidal field variation close to the synchrotron frequency to a transverse dipole located in a region of high dispersion. Since the time these

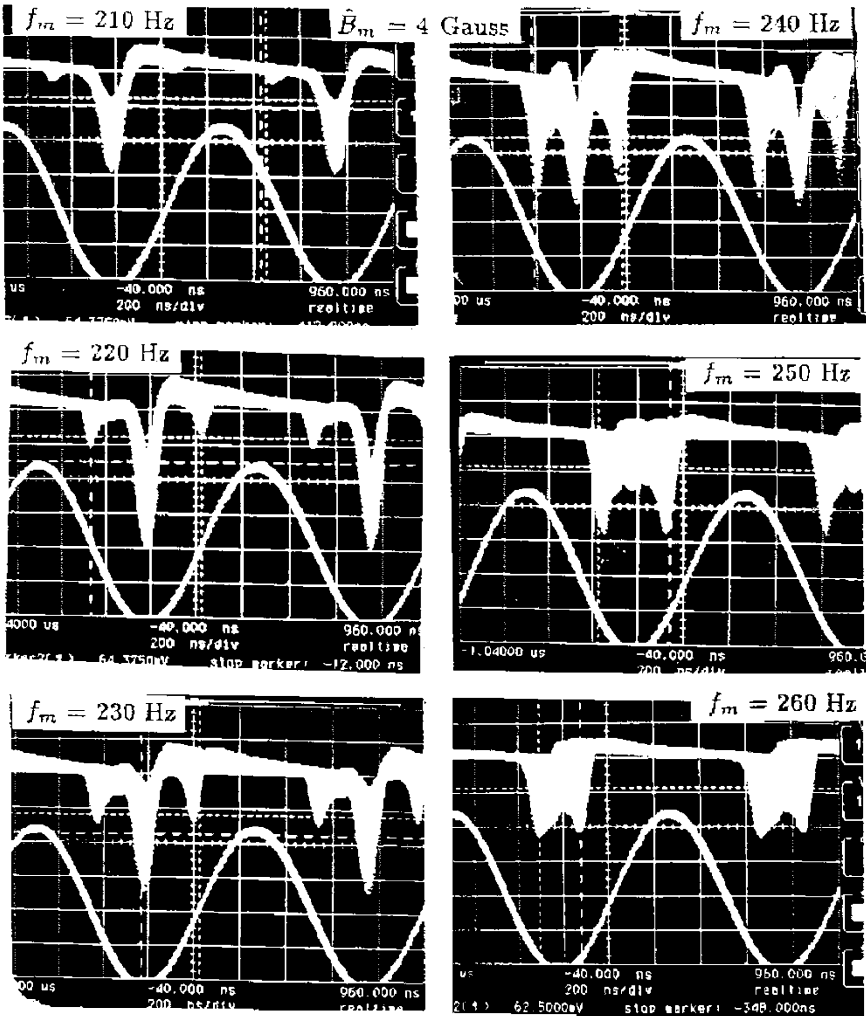

Fig. 8.9. Longitudinal beam profile observed using an oscilloscope (*top*) and the rf wave form (*bottom*) during rf modulation of proton bunches in the IUCF Cooler Ring (Courtesy S.Y. Lee, 1999)

data were taken, further experiments at the Advanced Light Source (ALS) with electron beams have included the use of streak camera for a more direct measurement of the evolution of the bunch length [25].

8.5 Harmonic Cavities

The use of additional rf cavities for longitudinal phase space manipulation has a variety of applications – we have already seen two such examples for bunch coalescing and splitting. Applications of harmonic cavities to reduce emittance growth when crossing transition (see Sect. 7.1) has been demonstrated at the Fermilab Main Ring [26, 27] and at BNL [28]. In this section we describe the use of harmonic cavities for lengthening the bunch. This approach has been adopted at various synchrotron light sources [29, 30] in order to either avoid intrabeam scattering effects and so increase the beam lifetime, or to increase the bunch length to avoid longitudinal beam instabilities, for example, at DAPHNE [31, 32] and as once proposed at LEP [33, 34].

Electron beam lifetimes at energies of the order 1 GeV or below may be dominated by large-angle intrabeam scattering otherwise known as Touschek [35] scattering. This process refers to single collisions between particles inside the same bunch, in which sufficient energy is transferred from the transverse to the longitudinal direction, such that particles are scattered outside of the ring energy acceptance. The energy acceptance is either equal to the height of the rf bucket, or given by a physical aperture at a position with large dispersion, whichever value is smaller.

In a somewhat simplified picture, the beam lifetime τ is approximately given by

$$\frac{1}{\tau} = \frac{\sigma c}{N} \int \rho^2 \, \mathrm{d}V \, , \tag{8.17}$$

where σ is the cross section for scattering beyond the energy acceptance, ρ is the bunch particle density, N the total number of particles in the bunch, and V represents the volume. For a constant beam energy and charge, the lifetime can be increased by increasing the bunch length and thus reducing the volume density ρ (nominally not coupled to the transverse emittances so that the transverse brightness remains unchanged). We note that a more accurate expression of the Touschek beam lifetime can be obtained by integrating the differential cross section over the momentum distribution of the beam, taking into account the correlations between position and momentum and between the different degrees of freedom as well as the variations of the optical functions around the ring, and always weighting with an appropriate convolution of two beam distribution functions [36, 37].

The increase of the bunch length using higher harmonic rf systems can be easily understood from Fig. 8.10. Here a third harmonic cavity is added to the primary rf such that the vector voltage seen by the beam is constant over the length of the bunch.

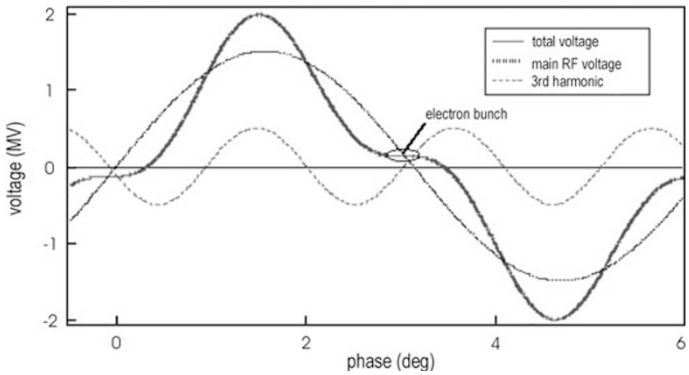

Fig. 8.10. Conceptual illustration of bunch lengthening with a higher harmonic cavity (Courtesy J. Byrd, 1999)

For electrons with nonzero synchronous phase, the total voltage is given by

$$V(t) = \hat{V}\left[\sin(\omega_{\rm rf}t + \phi_1) + k\sin\big(n(\omega_{\rm rf}t + \phi_h)\big)\right] , \tag{8.18}$$

where $\omega_{\rm rf}$ and $\hat{V}$ are the angular rf frequency and voltage of the fundamental rf, n is the ratio of higher harmonic to main accelerating cavity frequencies, k is the desired net voltage ratio for the two rf amplitudes, ϕ_1 is the phase of the primary rf system measured with respect to the zero crossing, and ϕ_n the harmonic phase. We assume that the bunch center arrives at time $t = 0$. Note that in (7.5) we defined the synchronous phase ϕ_s with respect to the crest of the rf, so that $\phi_s = \phi_1 - \pi/2$.

Then, we must have $eV(0) = U$, where U is the energy loss per turn (taken here to be dominated by synchrotron radiation). For optimum bunch lengthening both the slope and the curvature of the net voltage at the position of the bunch are zero, i.e.,

$$\left.\frac{{\rm d}V}{{\rm d}t}\right|_{t=0} = 0 \quad \text{and} \quad \left.\frac{{\rm d}^2V}{{\rm d}t^2}\right|_{t=0} = 0 . \tag{8.19}$$

The potential seen by the beam with and without a third harmonic rf system is shown in Fig. 8.11.

Equations (8.18) and (8.19) determine the optimum amplitude and phase of the harmonic cavity (see also [30]):

$$\begin{aligned} k^2 &= \frac{1}{n^2} - \frac{(U/(e\hat{V}))^2 n^2}{(n^2-1)^2} , \\ \tan\phi_h &= \frac{nU/(e\hat{V})}{\sqrt{(n^2-1)^2 - (n^2U/(e\hat{V}))^2}} , \\ \sin\phi_1 &= \frac{n^2}{n^2-1}\frac{U}{e\hat{V}} . \end{aligned} \tag{8.20}$$

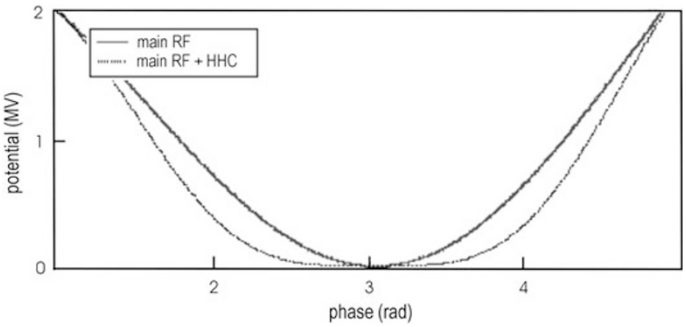

Fig. 8.11. Potential seen by circulating bunch with and without a harmonic cavity for the parameters of the ALS (Courtesy J. Byrd, 1999)

Simulations for the expected longitudinal density distribution are shown for the case of the ALS in Fig. 8.12.

The third harmonic RF system at the APS [29] consists of five single-cell copper 1.5 GHz cavities which are driven passively by the beam. With the resulting decreased peak charge density, an increase in beam lifetime exceeding a factor of two has resulted [38].

The beam current distribution, or fill pattern, has been shown to strongly affect the obtainable beam lifetimes [38] due to transient beam loading effects. Transient beam loading effects arise, because the beam is not a continuous current, but consists of bunches, and often these bunches are not uniformly distributed around the rings. A frequent beam pattern is one or several trains of equally spaced bunches, separated by 'gaps' without any bunches. Such gaps may be introduced, for example, to remove ions or photo-electrons, which otherwise are attracted and trapped by the beam electric field.

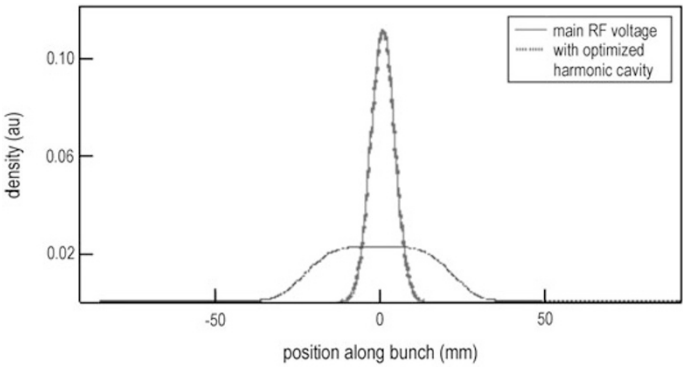

Fig. 8.12. Bunch length with and without a third harmonic cavity at the ALS (Courtesy J. Byrd, 1999)

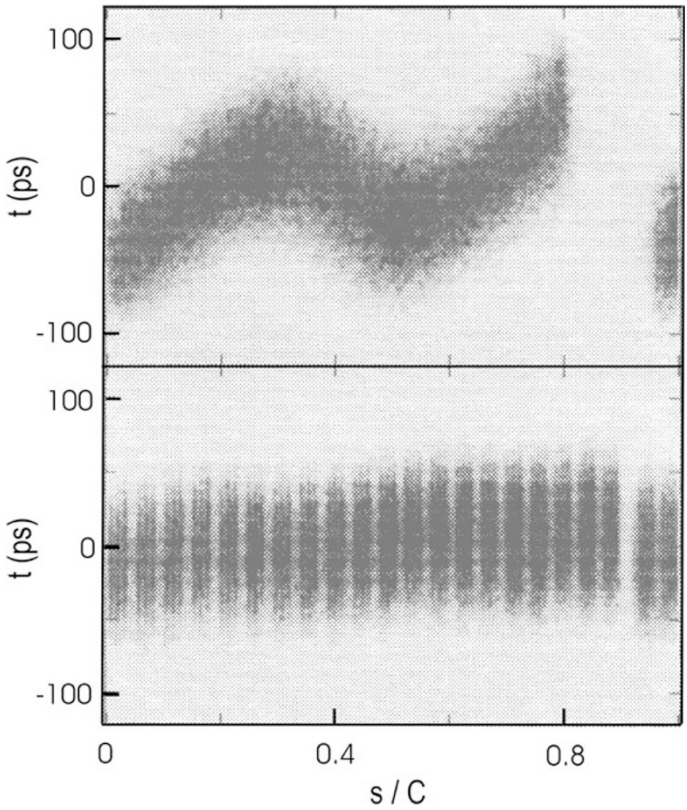

Fig. 8.13. Beam phase modulations measured at the ALS with a large (17% gap, *top*) and a small (2.4% gap, *bottom*) in the beam fill pattern (Courtesy J. Byrd, 2001)

Streak camera measurements of the longitudinal distribution versus bunch number are shown in Fig. 8.13 for the case of a large gap (17%) and for a small gap (2.4%) in the fill pattern. To date, simulation results of the variation in synchronous phase show good qualitative agreement with the measurements, yet do not explain the measured increases in the bunch length and beam lifetime [38].

The implications of phase variations along the fill pattern are two-fold. Most importantly, the gain in bunch-by-bunch feedback loops is reduced by such a phase variation. On the other hand, the increased interbunch or intrabunch phase spread contributes to increased Landau damping.

8.6 Energy Spread

As compared with the other 5 dimensions of a beam's phase space, the second moment corresponding to the beam energy spread is perhaps the most difficult to measure and control. In circular accelerators, lepton beams are naturally radiation damped to the limit of quantum fluctuations. Hadron beams on the other hand experience emittance dilutions particularly if subjected to internal targetry. For this reason various cooling mechanisms (see chapter 11) have been devised to combat large energy spreads.

Experience at both lepton and proton accelerators with high beam currents has shown that as the currents are increased, single-bunch instabilities due to longitudinal wake fields, dominated by the so-called microwave instability, can lead to an increase in the beam energy spread. Measurements at the SLC damping ring made with a wire scanner in a region of high dispersion in the extraction line are shown in Fig. 8.14. These measurements demonstrated a dramatic increase in the bunch energy spread beyond currents of about 1.5×10^{10} particles per bunch [39]. While relatively unimportant provided that the distribution remains stable from pulse-to-pulse, observations have shown that the increased energy spread is often associated with random turbulent bunch lengthening. Detailed analyses of this yet not fully understood phenomenon are beyond the scope of this book. Rather we will focus on methods for preserving, controlling, and minimizing the beam energy spread in linear accelerators and transport lines, assuming a constant incoming energy spread. We have already seen one example whereby the energy spread of a beam is increased as the bunch length is decreased using bunch precompression and bunch compression.

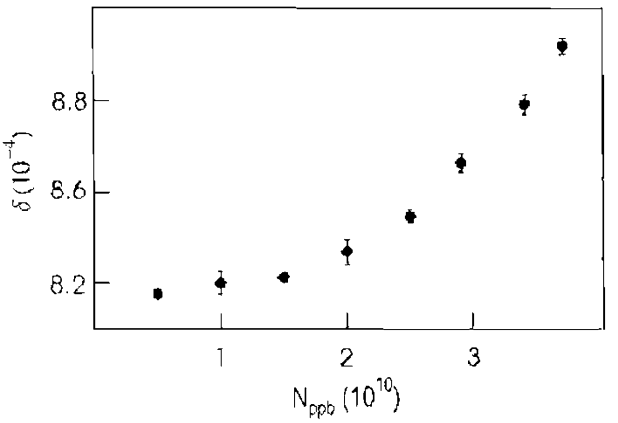

Fig. 8.14. Measured energy spread of beams exiting the SLAC electron damping ring as a function of beam current. The total cavity voltage in this measurement was 945 kV

In a linear accelerator, the energy of the particles with longitudinal density distribution $\rho(z)$ is a sum of the injected beam energy E_0, the energy gained in acceleration from each klystron ΔE_i, and the losses from longitudinal wake fields $W_\parallel$ [40, 41]:

$$E(z) = E_0 + \sum_{i=1}^{N_{\mathrm{klys}}} \left[\Delta E_i \cos(\phi_i + \phi(z)) + \Delta s_i N_b e \int_z^\infty {W^i}_\parallel(z' - z)\rho(z')\,\mathrm{d}z' \right], \tag{8.21}$$

where ϕ_i is the klystron phase (i.e., referring to the arrival time of the beam with respect to the crest of the rf in the ith acceleration section), $\phi(z) = 2\pi z/\lambda_{\mathrm{rf}}$, $\lambda_{\mathrm{rf}} = c/f_{\mathrm{rf}}$ the rf wavelength at frequency f_{rf}, N_b the bunch population, $W_\parallel(z)$ is the longitudinal wake function per unit length in units of eV/(Cm) as a function of particle distance z, $\rho(z)$ is the normalized longitudinal beam density, and Δs_i gives the distance between successive accelerating sections powered by different klystrons.

The energy spread of the bunch σ_E is obtained by averaging over the particle distribution after subtracting out the mean energy $\langle E \rangle$ of the bunch. Normalized to the mean energy of the bunch

$$\langle E \rangle = \int_{-\infty}^{\infty} E(z)\rho(z)\,\mathrm{d}z\,, \tag{8.22}$$

the relative energy spread is

$$\frac{\sigma_E}{E} = \frac{1}{\langle E \rangle} \left[\int_{-\infty}^{\infty} \big(E(z) - \langle E \rangle\big)^2 \rho(z)\,\mathrm{d}z \right]^{\frac{1}{2}}. \tag{8.23}$$

In the low-current limit, the beam does not take away any energy from the accelerating structures and the beam is placed on the crest of the rf wave to achieve both maximum acceleration and minimum energy spread within the bunch. At higher beam currents while invoking BNS damping, the klystrons in the first part of the linac are phased to impart relatively higher energy to the head of the bunch while in the latter part of the linac the klystrons are phased to restore the energy spread to less than the energy acceptance of the downstream target area or beam-delivery system.

At even higher bunch currents, one must carefully balance the two terms in square brackets in (8.21), that is cancel the energy variation along the bunch arising from the slope of the rf and that from the longitudinal wake field. Shown in Fig. 8.15 are sketches illustrating such cancellation. The effective rf gain representing the vector sum of all accelerating stations is plotted versus time (left) together with the projection of the charge distribution which shows the resultant energy spread of the bunch (right). At low current, a bunch placed on crest has minimum energy spread. Off crest, a position-energy correlation is introduced and the energy spread is increased. At high current, due to longitudinal wake field, or *beam loading*, a bunch placed on crest has a large energy spread. For short, high intensity bunches, the energy spread may

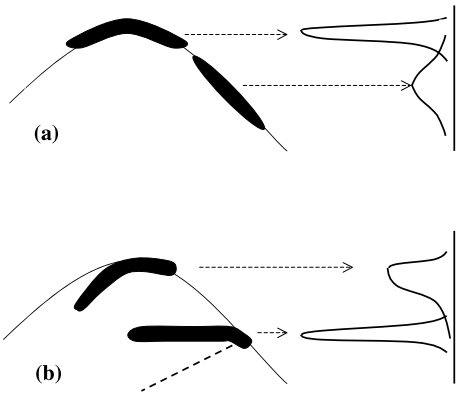

Fig. 8.15. Effective energy gain (*left*) and energy spread (*right*) for low (**a**) and high (**b**) current bunches illustrating optimum phasing of the rf structures for minimum energy spread

be minimized by placing the beam off-crest as shown. In this case the beam-induced wake field (dotted line) exactly cancels the slope of the rf across the bunch.

The energy spread can also be modified by changing the longitudinal beam distribution in the linac. A clever technique of adjusting the bunch shape in the SLC linac consisted in raising or lowering the compressor voltage, relative to the ideal case of maximum compression (see Sect. 8.1). These two modes of operation are called overcompression or undercompression, respectively. Although the same rms bunch length can be obtained with either mode, the shape of the bunch is quite different, which is partly due to an initial distortion caused by impedance effects in the upstream damping ring. Operation with overcompression produced the desired forward-peaked distribution [42] and was used to avoid undesirable energy tails at the end of the linac [43] (see also Fig. 8.20).

Simulation results using (8.3) are shown in Fig. 8.16. While perhaps nonintuitive, simply by 'overcompressing' the bunch, the tails in the energy spread distribution could be eliminated without diluting the longitudinal beam emittance. Measurements of the beam at the end of the SLC linac in a dispersive region are shown [43] in Fig. 8.17 with undercompression (left) and with overcompression (right). The absence of the low energy tails in the latter case justified the routine use of over-compressed beams at the SLC.

In linear accelerators with high current bunches the longitudinal density profile can be further adjusted (so-called bunch shaping) to minimize transverse emittance dilutions arising from short-range wake fields and/or dispersion. This is particularly useful since the outgoing energy spread, and especially energy 'tails', often cause even further emittance dilutions downstream due to chromatic aberrations in the final focus systems.

Minimization of the energy spread depends critically on the single-bunch charge. In the single particle approximation, the energy gained through an accelerating structure is

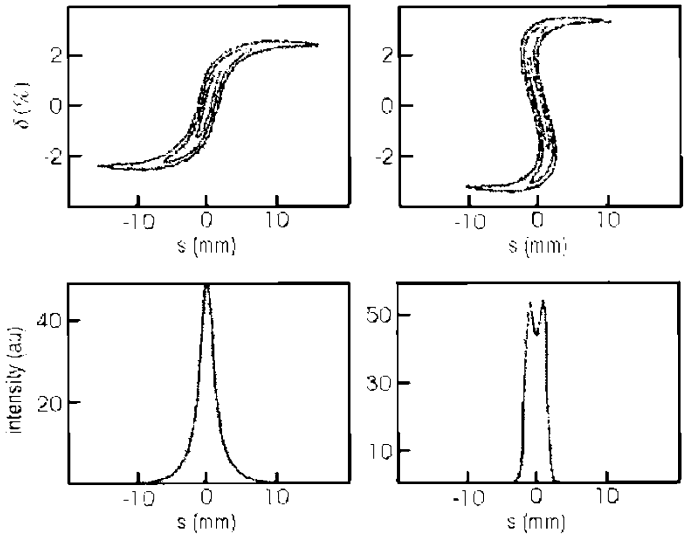

Fig. 8.16. Longitudinal phase space (*top*) and projections onto time axis (*bottom*) with undercompression (*left*) and with overcompression (*right*) (Courtesy F.-J. Decker, 1999)

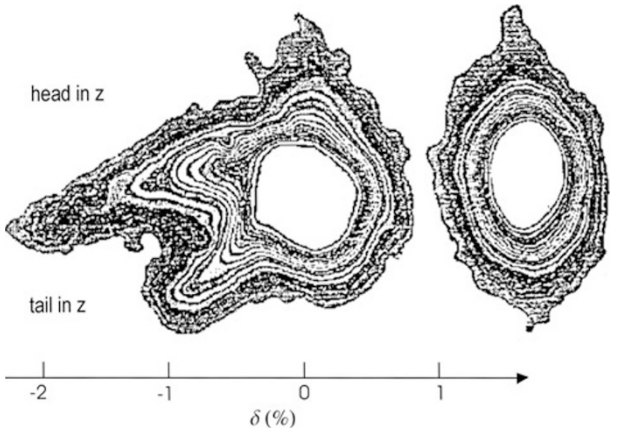

Fig. 8.17. Measurements of the beam profile at a dispersive location at low compressor voltage (*left*) and with bunch overcompression (*right*) (Courtesy F.J. Decker, 2000)

$$eV = E_k L_k \cos\phi_k \ , \tag{8.24}$$

where E_k is the accelerating gradient in units of MeV/m, L_k is the length of the accelerating region, and ϕ_k is the time-like variable representing the phase of the particle relative to the crest of the rf. The magnitude of E_k

and the definition of the phase ϕ_k include possible effects of klystron phase errors.

For a bunch of particles, the energy seen by a given particle is reduced due to loading of the accelerating structure by leading particles within the bunch. Letting ϕ_0 represent the phase at the head of the bunch with respect to the crest of the rf, the total energy gain at the end of the linac becomes

$$eV(\phi_k) = E_k L_k \cos\phi_k + N_b e \int_0^{\phi_0-\phi_k} \rho(\phi') W_\parallel(\phi_0 - \phi_k - \phi')\,\mathrm{d}\phi' \,, \qquad (8.25)$$

where $\rho(\phi')$ represents the bunch charge distribution, and $W_\parallel$ is the wake function for the entire accelerator and is given by the product of the single-bunch wake field times the number of accelerating structures.

Minimum energy spread within the bunch requires that $V(\phi_k)$ is independent of ϕ_k; that is

$$\frac{\partial V(\phi_k)}{\partial \phi_k} = 0 \,. \qquad (8.26)$$

It has been shown [42] that there exists a solution for the bunch charge distribution $\rho(\phi)$ which satisfies this criterion, and which can be obtained by numerically solving

$$\rho(x) = \frac{E_k L_k}{W_\parallel(0)} \sin\left(\phi_0 - \tilde{\phi}\right) + N_b e \int_0^{\tilde{\phi}} \frac{\frac{\partial W_\parallel}{\partial \tilde{\phi}}\left(\tilde{\phi} - \phi'\right)\rho(\phi')}{W_\parallel(0)}\,\mathrm{d}\phi' \,, \qquad (8.27)$$

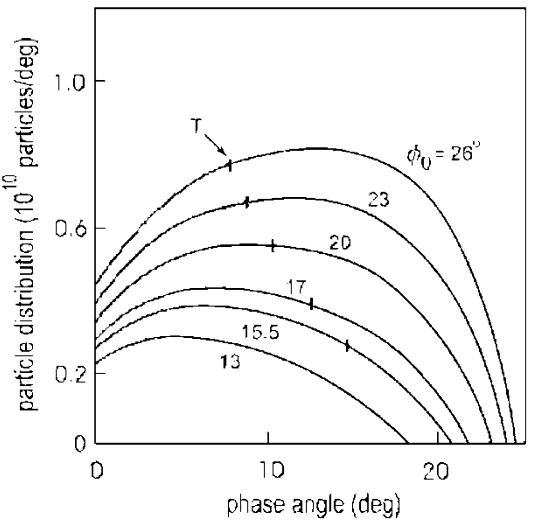

Fig. 8.18. Optimum bunch shape for beam loading compensation in the SLC linac. The bunch head is on the left (Courtesy G. Loew, 1999)

where $\tilde{\phi} \equiv (\phi_0 - \phi_k)$. The interpretation of (8.27) is quite analogous to that shown in Fig. 8.10. Only in this case, the voltage provided by the higher harmonic cavity is replaced by the decelerating voltage induced by beam loading of the leading particles within the bunch.

The solution given in (8.27) is shown in Fig. 8.18 for the SLC linac. The horizontal axis shows the phase angle of particles within the bunch measured with respect to ϕ_0 with the leading particles located at zero phase angle. The different curves labelled by ϕ_0 designate the position of the head of the bunch with respect to the crest of the rf in units of degrees, and the points marked 'T' indicate where the integrated bunch charge reaches the design single bunch population of $N_b = 5 \times 10^{10}$ particles per bunch. As can be seen, for minimum energy spread, the preferred charge distributions tend in general to have a steeply rising edge.

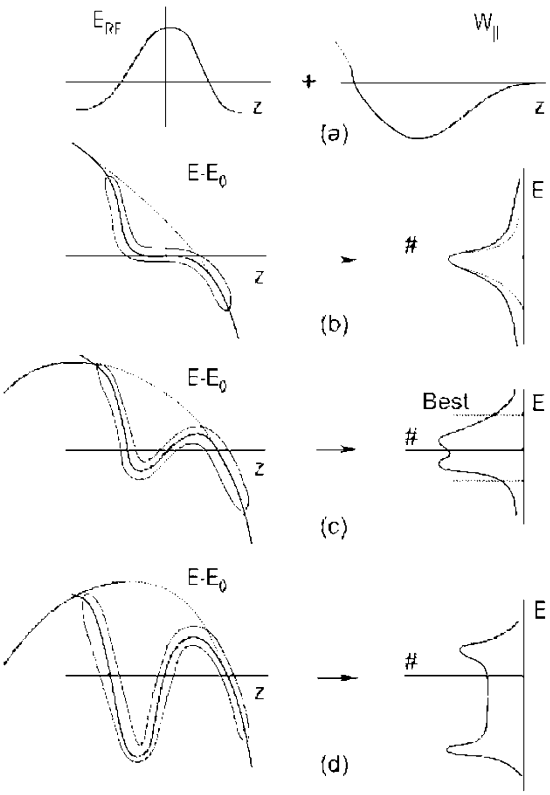

Fig. 8.19. Conceptual illustration for optimizing the relative phase of the beam for the case of very long bunches. The accelerating field E_{rf} and the longitudinal wake field $W_{\|}$ are shown in (**a**). The longitudinal profiles and their projections onto the energy axes are shown for different relative phases (between the beam and the rf wave) in (**b**)–(**d**) (Courtesy J. Seeman, 1999)

The tradeoff between bunch length and energy spread in a linear accelerator is illustrated in Fig. 8.19, which shows the effect of the combined voltages from the power source E_{RF} and the longitudinal wake field $W_{\|}$. On the left is depicted the longitudinal phase space of a long bunch while the projection onto the energy axis is given on the right. In the limit of long bunches one can see that a 'double-horned' distribution produces the minimum rms energy spread.

Measured energy spread profiles taken at the end of the SLAC linac are shown in Fig. 8.20. A wire scanner located in a dispersive region of a downstream transport line was used to measure the profile σ_w. The energy spread σ_δ was inferred by subtracting out, in quadrature, the contribution from the betatron beam size $\sigma_\beta = \sqrt{\epsilon_x \beta_x}$:

$$\sigma_\delta = \sqrt{{\sigma_w}^2 - {\sigma_\beta}^2} \,. \tag{8.28}$$

The angle ϕ denoted in the figure shows the BNS phase angle at the time of the measurement. These data show clearly the effects of not only misphasing the linac, but the additive contributions of the short-range longitudinal wake field and have been used together with simulation [44, 45] to determine the longitudinal bunch distribution at the SLC.

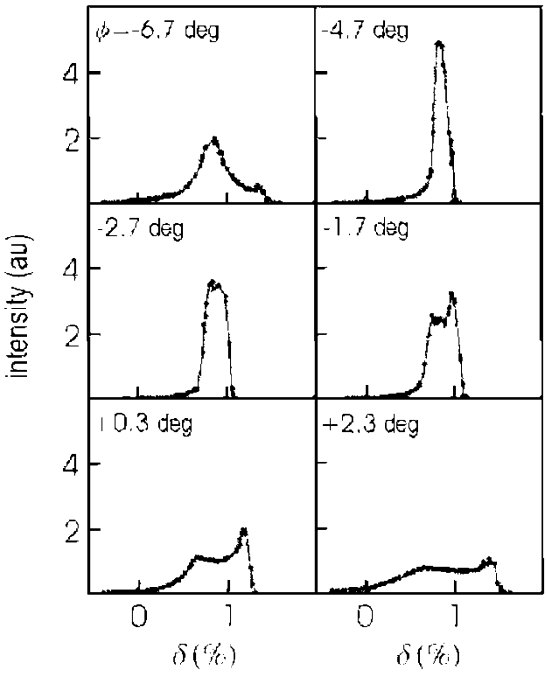

Fig. 8.20. Energy spread measurements taken at the end of the SLAC linac for different BNS phases (ϕ) (Courtesy K. Bane, 1999)

8.7 Energy Compression

The energy spread of a single bunch can be made smaller (at the expense of increased bunch length) using reverse application of a bunch length compressor. In this case, the beam first passes through a region with an energy-dependent path length, in which the particles of different energy are separated in time. Following this is an accelerating section which decelerates and accelerates the high and low energy particles, respectively. Energy compression for single bunches was designed and implemented [46] for the positron transport line into the SLAC positron damping ring. The net increase in particle yield was observed to be about 10%.

8.8 Beam Loading and Long-Range Wake Fields

In the quest for obtaining ever-increasing total beam currents, both newly constructed and future accelerators have in common bunch trains consisting of multiple, closely spaced, high-current bunches. In both linear and circular accelerators this may lead to a relative phase shift between the bunches of a bunch train (an example was shown in Fig. 8.13).

When a beam passes through an accelerating cavity, it induces a voltage $V_{b,m}$ in each mode m of the cavity. The induced voltage is always retarding; that is, the beam-induced voltage always acts to decelerate the beam. Expressed another way, the beam always takes energy away from the cavity. This is refered to as beam loading.

The fundamental theorem of beam loading [47] is relevant on short time scales (i.e., for a single pass through an accelerating cavity). The theorem states that the voltage that a test particle would experience when trailing a (point) source particle at time $t_0 > 0$ is exactly twice its beam induced voltage at $t_0 = 0$. More generally, the induced voltage, or wake potential, V_δ is given by

$$\begin{aligned} V_\delta(t_0) &= 0 \quad \text{for} \quad t_0 < 0 \\ &= -kq \quad \text{for} \quad t_0 = 0 \\ &= -2kqe^{-\frac{t_0}{\tau_f}} \cos\omega_{\mathrm{rf}} t_0 \quad \text{for} \quad t_0 > 0\,, \end{aligned} \tag{8.29}$$

where $\tau_f = 2Q/\omega_{\mathrm{rf}}$ is the fill time of the cavity and Q is the cavity quality factor. Here, the variable

$$k = \frac{\omega}{2}\left(\frac{R}{Q}\right) \tag{8.30}$$

is called the loss parameter which tends to be determined by the structure geometry close to the beam. In practice, k is often calculated for each cavity mode using numerical programs, e.g., MAFIA. The wake potential describes

the electromagnetic field that the point-like beam generates as it interacts with its surroundings and how this field acts back on the beam, thus perturbing its motion.

We consider next the effect of multi-bunch or multi-turn beam loading, which is caused by the interaction of the beam with the fundamental accelerating mode of the rf cavity on successive bunch passages. In addition, there is also a short-range effect, which consists of the superposition of many higher-order cavity modes. These higher-order modes are usually damped, so that the short-range wake field quickly decays. The fundamental mode on the other hand is used for the acceleration, and, hence, it necessarily exhibits a weak damping, or a high Q value.

In a circular accelerator containing a single accelerating cavity and a single particle bunch, the steady-state ($t \gg \tau_f$) beam-induced voltage V_b is given by summing over the contribution from all previous turns. For short bunches, using (8.29) with $T_{\rm rev}$ denoting the revolution frequency,

$$\begin{aligned} V_b &= -kq - 2kq \sum_{n=1}^{\infty} e^{-\frac{t_0}{\tau_f}} \cos\omega t_o \delta(t_0 - nT_{\rm rev}) \\ &= -2kq \left[\sum_{n=0}^{\infty} e^{-\frac{t_0}{\tau_f}} \cos\omega t_o + \frac{1}{2} \right] \delta(t_0 - nT_{\rm rev}) \\ &= -2kq \left[\sum_{n=0}^{\infty} e^{-\frac{nT_{\rm rev}}{\tau_f}} \cos n\omega T_{\rm rev} + \frac{1}{2} \right] . \end{aligned} \tag{8.31}$$

Driving the cavity near its resonance frequency, i.e., taking $\omega = \omega_{\rm rf}$, and noting that $\cos(n\omega T_{\rm rev}) = 1$ for all n, we can simplify this expression and find

$$\begin{aligned} V_b &= -2kq \left[\sum_{n=0}^{\infty} e^{-\frac{n\omega_{\rm rf}}{2Q} T_{\rm rev}} + \frac{1}{2} \right] \\ &= -2kq \left[\frac{1}{1 - e^{-\frac{n\omega_{\rm rf}}{2Q} T_{\rm rev}}} + \frac{1}{2} \right] . \end{aligned} \tag{8.32}$$

Neglecting the small self-loading term (factor 1/2), and applying

$$\frac{1}{1 - e^{-x}} \approx \frac{1}{x} \quad \text{for} \quad x = \frac{\omega_{\rm rf} T_{\rm rev}}{2Q} \ll 1 , \tag{8.33}$$

we then obtain

$$\begin{aligned} V_b &= -2kq \left(\frac{2Q}{\omega_{\rm rf} T_{\rm rev}} \right) , \quad k = \frac{\omega_0}{2} \left(\frac{R}{Q} \right) \\ &= -2q f_{\rm rev} R \\ &= -I_b R . \end{aligned} \tag{8.34}$$

This simple result shows that with the cavity tuned to resonance, the beam-induced voltage is simply given by the beam current at the resonance frequency ($I_b = 2I_{dc}$) times the cavity impedance. (Note that this is the loaded impedance, i.e., the combined impedances of the cavities, the connecting wave guides and rf power source, and the possible influence of rf feedback loops. The minus sign, again, indicates that the beam takes energy away from the accelerating cavity.

Application of (8.29 and 8.34) to the transport of high current particle beams is a subject of great interest in modern accelerators. In the extreme short-range limit ($t < \sigma_z \omega / c$), the variable t_0 may represent the time interval between particles within a single bunch in which case, by causality, the charge q represents the charge of all preceding *particles within the bunch*. As the beam current is increased, eventually, as many experimental and theoretical studies have shown, the ensuing motion can become unstable. BNS damping in a linac is used, for example, to avoid the beam breakup instability associated with short-range wake fields.

At the SLC high beam currents were achieved using BNS damping and single, widely spaced bunches each of high charge (about 4×10^{10} particles per bunch). At such high bunch charges, the effects of long-range wake fields ($t \sim \tau_{bb}$, where τ_{bb} is the spacing between bunches) were also observed. Shown in Fig. 8.21 is a measurement [48] showing the orbit oscillation induced after changing τ_{bb} by 1 (of about 170) rf buckets. Using similar measurements with variable bunch spacings, the frequency of the driving mode could be roughly determined and compared with numerical models. Interestingly, the simplicity of the SLC (FODO) lattice and the different sign of accelerated particle species was such that the deflections due to the higher-order wake fields added coherently along the SLC linac. To minimize this resonant build-up, the symmetry of the focussing was changed using a so-called 'split-tune' lattice [48].

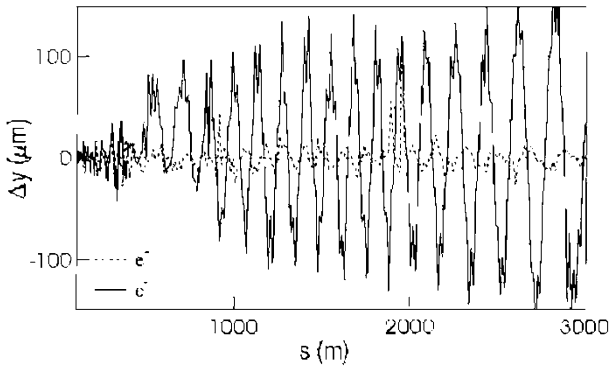

Fig. 8.21. Measured vertical difference orbit of the trailing electron bunch (*solid line*) after displacement of the leading positron bunch by 1 rf bucket (*dashed line*) in the SLC linac

Here the horizontal and vertical phase advances were changed so as not to be equal. In this way, resonant excitation of the leading positron bunch had less influence on the trajectory of the trailing electron bunch (the horizontal phase advance of the electrons equals the vertical phase advance of the positrons). The pulse-by-pulse jitter of the electron bunch was reduced [48] by about 15% horizontally (from $0.4\sigma_x$ to about $0.35\sigma_x$) and 30% vertically (from $0.75\sigma_y$ to about $0.50\sigma_y$).

The preferred way nowadays to achieve even higher beam currents, while avoiding intrabunch beam instabilities arising from increased single-bunch beam currents, uses multiple bunches (often called a bunch train) each with lower single-bunch beam currents. In this case, t_0 in (8.29) refers to the spacing between appropriate bunches. Now the beam-induced voltage experienced by a particular bunch is given by the sum of the voltages induced by *all preceding bunches* each obtained by evaluating (8.29) at the appropriate time $t_0 = N\tau_{bb}$, where N denotes the number of bunch spacings to the preceeding bunch of interest. In future linear collider designs with multi-bunch beams, research and development in the design of the accelerating structures aims towards minimizing the strength of the offending modes. An example,

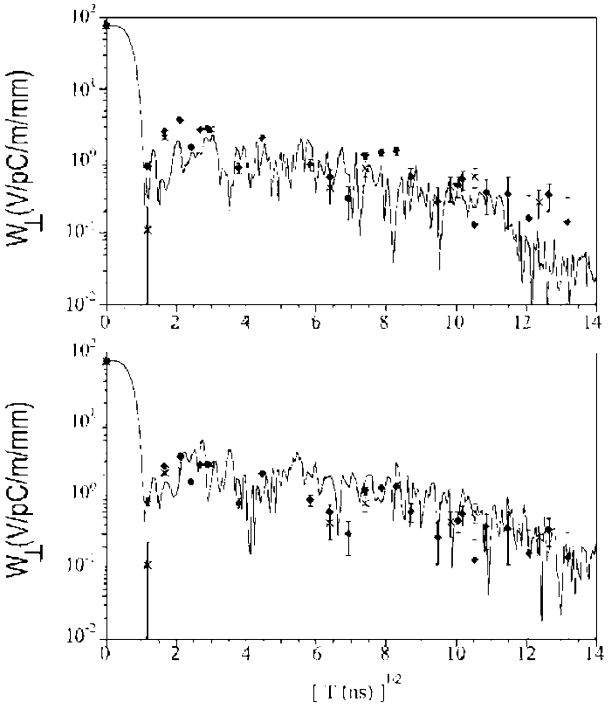

Fig. 8.22. Horizontal (*crosses*) and vertical (*diamonds*) wake field measurements and predictions (*solid lines*) in the X-band structure test at ASSET at SLAC (courtesy C. Adolphsen, 2002)

from the Accelerator Structure Setup (ASSET) facility at SLAC, is shown in Fig. 8.22 [49]. Here again, the spacing between the drive and trailing bunches was varied and the particle orbits were recorded and analyzed to give deflection seen by the trailing bunch and so determine the strength of the transverse wake field.

In existing circular accelerators operating already with high current, multi-bunch beams, much effort has been devoted to carefully developing and testing new cavity and feedback designs. At KEKB novel ARES [50] energy-storage cavities, super conducting cavities, and multi-bunch feedback are used to minimize the effect of wake fields. At PEP2 higher-order mode dampers and both multi-bunch and rf feedback are used. While bunch-to-

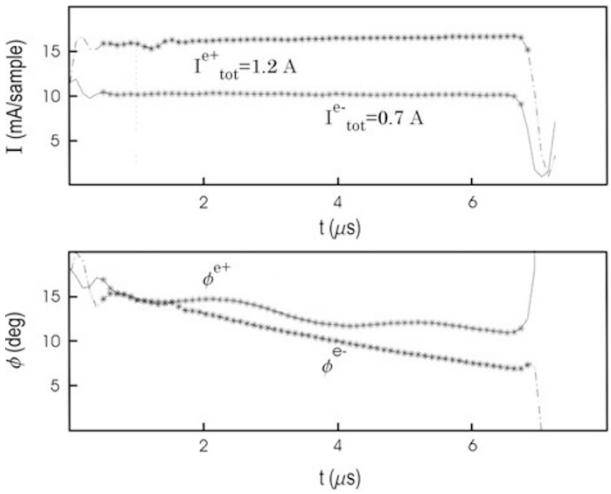

Fig. 8.23. Measured beam currents and beam phases for the PEP-II electron and positron beams (Courtesy P. Corredoura, 2000)

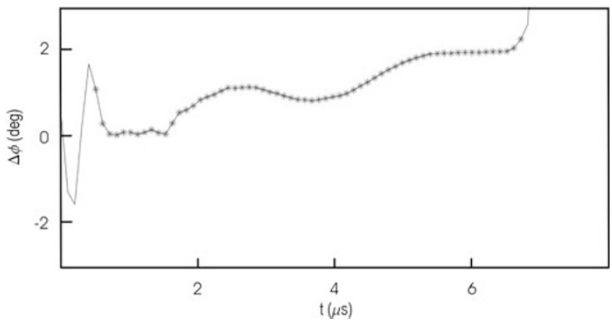

Fig. 8.24. Measured phase difference between the PEP-II electron (HER) and positron (LER) beams (Courtesy P. Corredoura, 2000)

bunch stability at both accelerators is excellent, even at total currents in the range of Amperes, beam loading is still an issue.

As an example, measured phase changes across the bunch fill patterns are shown in Fig. 8.23 from the PEP2 B-factory. The bunch distribution was uniform with a 5% gap in the fill pattern. This nonuniformity in the fill results in a change in cavity voltage along the bunch train and, from (7.5), a change in synchronous phase. This phase variation leads to a reduction in gain of the feedback loops. In addition, the phase difference between the two trains must be minimized to ensure the desired (longitudinal) collision point and hence the highest possible luminosity. The difference in the phase transients of the two beams is shown in Fig. 8.24.

8.9 Multi-Bunch Energy Compensation

Two methods, known as Δf and Δt compensation have been proposed to combat multibunch phase transients in linear accelerators. Shown in Fig. 8.25 is the principle of Δt compensation [51]. Here the voltage V_k represents the voltage response of a finite bandwidth accelerating structure to a step function input pulse. The lower curve represents the beam-induced voltage V_b of the entire bunch train. By injecting the beam prior to the time the linac structure is at peak voltage, the vector sum V_k+V_b is observed to be flat over the duration of the bunch train. The projected energy spread is therefore minimized and the phase relationship between the bunches is constant.

The principle of the Δf compensation is illustrated [52] in Fig. 8.26. In this design from the ATF in Japan, some fraction of the many accelerating structures are slightly detuned by $\pm\delta f$. The different bunches therefore obtain a different energy gain which depends on their location within the train.

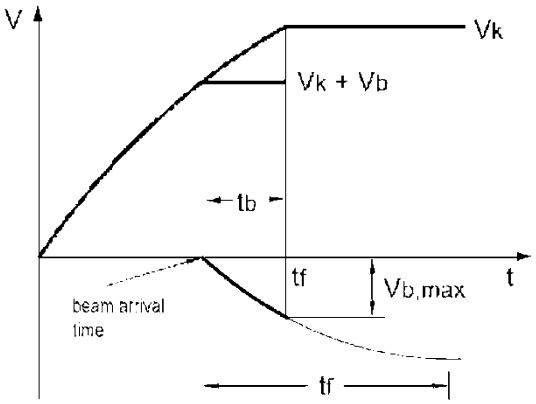

Fig. 8.25. Conceptual diagram illustrating multi-bunch, Δt beam loading and energy compensation

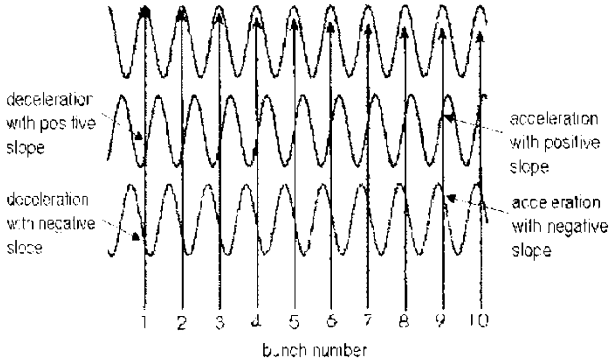

Fig. 8.26. Conceptual diagram illustrating multi-bunch, Δf beam loading and energy compensation [53] (Courtesy J. Urakawa, 1999)

With some structures detuned by $+\delta f$ and some by $-\delta f$ the position-energy correlations introduced by the slope of the rf cancels. In this way, not only is the projected energy spread along the bunch train minimized, but the energy spread of each bunch is also preserved.

Beam loading compensaton using the Δt method may be advantageous since the correction may be applied locally at each accelerating section. On the other hand it is anticipated [51] that about 10% more power is required relative to the Δf compensation scheme.

8.10 Damping Partition Number Change via RF Frequency Shift

The generation of small emittance beams is a key issue for synchrotron light sources, collider rings, and for future linear colliders. Dedicated accelerators have been designed to produce such beams, but techniques to further reduce the design emittances would yield immediate improvements. At injection into such accelerators, the transverse beam emittances are large and often fill a large fraction of the dynamic aperture. For lepton beams, at later times after the beam has radiation damped, the horizontal damping time and equilibrium emittance may be reduced by shifting the rf frequency, such that the particle orbit moves inwards. By passing off-center through the quadrupoles in regions of nonzero dispersion, the horizontal partition number J_x is changed. This reduces both the horizontal damping time and equilibrium emittance. In addition, to the extent that the vertical emittance is determined by betatron coupling, the reduction in horizontal emittance may be accompanied by a corresponding reduction in vertical emittance.

The horizontal damping time and beam emittance are both inversely proportional to the horizontal partition number $J_x = 1 - \mathcal{D}$, where [54]

$$\mathcal{D} = \frac{\int D_x G(G^2 + 2k)\,\mathrm{d}s}{\int G^2\,\mathrm{d}s} \,. \tag{8.35}$$

Here D_x is the horizontal dispersion, $G = 1/\rho$ and k describe the inverse bending radius in m^{-1} and the quadrupole focusing gradient m^{-2}, respectively, and the integrals are evaluated around the ring circumference. For the non-combined function magnets in the SLC damping ring, $Gk \approx 0$.

For a beam orbit offset Δx in the quadrupoles, the change in $\mathcal{D}$ is given approximately by

$$\Delta\mathcal{D} \approx \frac{2k^2 D_{x,q} L_q N_q}{2\pi/\rho} \Delta x \,, \tag{8.36}$$

where $k = \frac{ec}{E}(\frac{\partial B}{\partial x})$ with $e = 1.6 \times 10^{-19}$ C, $c = 3 \times 10^{10}$ m/s, $E = 1.19$ GeV, ρ is the local bending radius, $D_{x,q}$ is the dispersion at the quadrupoles, and L_q and N_q are respectively the quadrupole length and number of quadrupoles.

The orbit may be offset in the quadrupoles by either changing the accelerating frequency or by physically displacing the magnet support girders. Emittance optimization using the accelerating frequency has been used in $\mathrm{e}^+\mathrm{e}^-$ storage rings previously [55] and is used routinely at LEP [56]. The effect of changing the geometric ring circumference was already dicussed in Sect. 4.3.1. The circumference adjustment is applicable provided that the transverse acceptance is not limited and that the injected beam energy spread is small compared to the energy acceptance. At the SLC, the electron damping ring was 'stretched' [57] in 1992 by 9 mm for a 15% increase in J_x. In doing so, the energy aperture at injection was reduced yet without any loss in transmitted beam current. For the case of the positron damping ring, the incoming beam filled the entire aperture so stretching the accelerator was not an option.

Shown in Fig. 8.27 is a calculation of the horizontal emittance $\gamma\epsilon_x$ as a function of time for 4 different frequency offsets for the case of the SLC damping rings. It is assumed that the beam is injected at the nominal rf frequency of 714 MHz with an initial emittance of 20×10^{-5} m-r. The accelerating frequency is increased after 1 ms (dashed line) for which the longitudinal emittance has damped by about a factor of 2. The simulations (using SAD [58]) with a trapezoidal approximation for the bending magnet fringe fields show a half unit reduction (i.e., 15–20%) in normalized emittance with a 100 kHz frequency change, while the damping time reduces from 3.4 ms to 3.0 ms.

At storage rings and colliders, there is no tight tolerance on maintaining the desired rf frequency. In a damping ring, the time required to reset the frequency and relock the beam phase to the desired extraction phase is critical since the frequency must be ramped back to nominal just before extraction in order not to introduce any energy and/or phase errors in downstream subsystems (in our example, the SLC bunch compressor and the SLC linac). Minimizing this time [59] is critical since reverting to the nominal rf frequency is associated with corresponding antidamping of the beam.

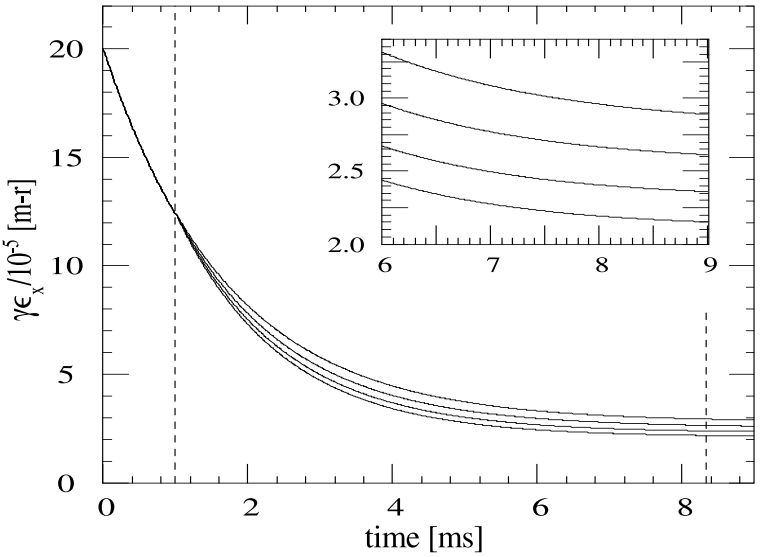

Fig. 8.27. Normalized horizontal beam emittance as a function of store time for different frequency shifts calculated for the SLC damping rings. The full store time is shown with an expanded view near beam extraction at 8.33 ms shown in the *insert*. The *curves*, when viewed *from top to bottom*, correspond to frequency shifts of 0, 50, 100, and 150 kHz, respectively

As a practical point, with a change in accelerating frequency, the accelerating cavities are detuned by an amount characterized by the tuning angle ϕ_z which is given by

$$\phi_z = \tan^{-1}\left[2Q\left(\frac{f_0 - f_{\rm rf}}{f_0}\right)\right] , \tag{8.37}$$

where Q is the loaded cavity quality factor, f_0 is the resonant frequency of the cavity, and $f_{\rm rf}$ is the frequency of the applied rf. With the cavity tuners *fixed*, the new tuning angle $\phi_z{}'$ corresponding to the new applied rf frequency $f_{\rm rf}{}' = f_{\rm rf} + \delta f_{\rm rf}$ is given by

$$\tan\phi_z{}' = 2Q\left[1 - (1 - \frac{1}{2Q}\tan\phi_z)\frac{f_{\rm rf}{}'}{f_{\rm rf}}\right] . \tag{8.38}$$

An example is shown in Fig. 8.28(a). Typically, the tuning angle is set for minimum reflected power:

$$\phi_z|_{\phi_l=0} = -\frac{I_b R}{\hat{V}}\sin\phi_b , \tag{8.39}$$

where I_b is twice the dc beam current, R is the total loaded impedance, $\hat{V}$ is the total cavity voltage in units of V, and ϕ_b is the synchronous beam phase

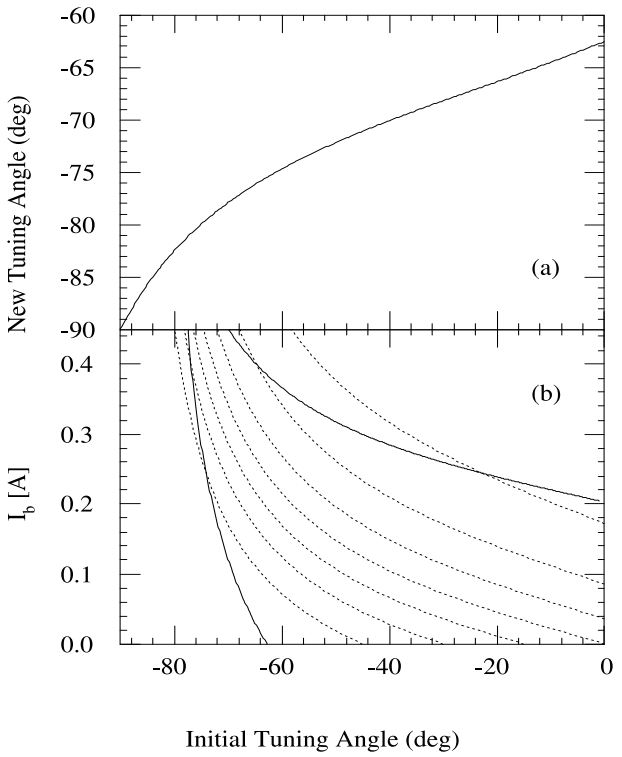

Fig. 8.28. Cavity tuning considerations. The initial and final tuning angles at $f_{\rm rf}$ and $f_{\rm rf}{}' = f_{\rm rf} + 100$ kHz, respectively, are shown in (**a**). The stability boundary for cavity voltage regulation at 600 kV is given by the *two solid curves* in (**b**). The *dashed curves* show the loading angle ϕ_l which is measured and regulated by the tuner feedback loops. At zero beam current the loading angle is equal to the tuning angle

measured with respect to the crest of the accelerating rf. The loading angle ϕ_l is related to the tuning angle ϕ_z by

$$\tan\phi_z = \left(1 + \frac{I_b R}{V_c}\cos\phi_b\right)\tan\phi_l - \frac{I_b R}{V_c}\ \sin\phi_b\ . \tag{8.40}$$

In the case of the SLC, at zero beam current the cavity detuning exceeded the power capabilities of the power source as indicated by the lower solid curve in Fig. 8.28(b).

Assuming sufficient frequency aperture, which may be restricted, e.g., by transverse betatron resonances that can be encountered during the frequency ramp with nonzero chromaticity or by a physical aperture in a region with nonzero dispersion, the maximum frequency change may be limited by either available rf power as discussed above or by the damping poles [60] at which the damping rate becomes zero.

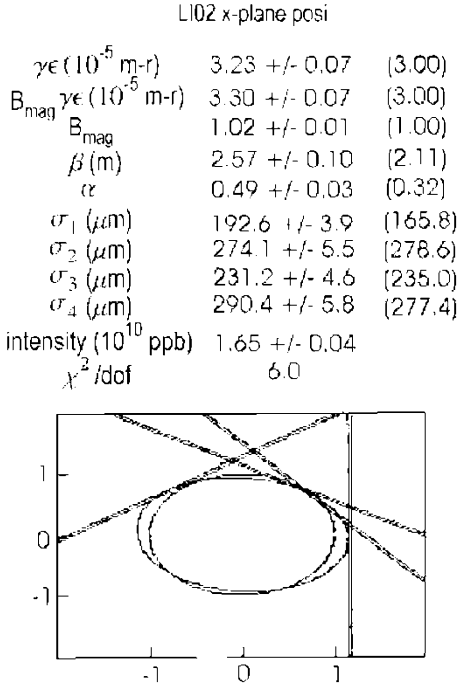

Fig. 8.29. Nominal emittance at injection to the SLC linac without an rf frequency shift in the upstream damping ring. The measured normalized emittance was 3.30 ± 0.07 m

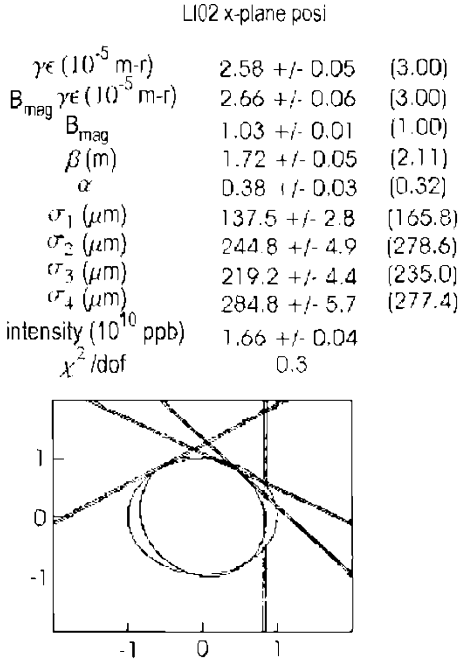

Fig. 8.30. Normalized emittance measurement at injection to the SLC linac with a 62.5 kHz frequency shift in the upstream damping ring. The normalized emittance was reduced from 3.30 ± 0.07 m to 2.66 ± 0.06 m

Measurements [61] showing the effect of a frequency ramp in the SLC positron ring are given in Figs. 8.29 and 8.30. In this experiment, the downstream compressor was turned off in order to more cleanly detect the effect of the frequency shift on the beam emittance. From Fig. 8.30, with a 62.5 kHz shift, the reduction in normalized emittance was from 3.30 ± 0.07 m to 2.66 ± 0.06 m. For the electron damping ring, the frequency shift reduced the horizontal normalized emittance from 3.22 ± 0.08 m to 2.93 ± 0.07 m. We expected that the emittances at the entrance of the final focus would be reduced by a similar amount to $\gamma\epsilon_x = 5.2 \times 10^{-5}$ m and $\gamma\epsilon_y = 1.1 \times 10^{-5}$ m, and, using the 1997 SLC interaction point parameters with rms angular divergences of $\theta_x = 450$ μrad and $\theta_y = 250$ μrad, the corresponding rms beam sizes at the collision point were estimated to be $\sigma_x = 1.3$ μm and $\sigma_y = 0.5$ μm. With a 1 mm bunch length and 4×10^{10} particles per bunch, the luminosity was computed by the code Guinea-Pig [62] to be 4.3×10^{32} m^{-2} per collision. This corresponded to an estimated increase of over 40% in luminosity by application of the frequency shift in the damping rings. Unfortunately, no rigorous study was undertaken to experimentally quantify the effect of the rf frequency shift on the SLC luminosity.

Decreasing the beam emittance by changing the damping partition numbers is also part of the HERA luminosity upgrade [63]. To maintain matched beam sizes, with a reduced proton beam size resulting from the modified optics at the interaction points of HERA, the electron beam size must be reduced. The approach that was taken is twofold: stronger focussing in the arcs, which reduces the horizontal equilibrium emittance, and a +200 Hz rf frequency shift, which changes the damping partition numbers.

Exercises

8.1 Phase Tolerances in a Bunch Compressor

Consider a 1.2 GeV electron beam passing through a 2856 MHz compressor cavity and a transport line with $R_{56} = -0.6$ m. Sketch the error in the final phase as a function of injection phase error for different accelerating voltages. At which compressor voltage is the final beam phase, behind the compressor region, minimially sensitive to initial phase errors?

8.2 Bunch Precompression

a) Describe (or sketch) the motion of the beam centroid in longitudinal phase space for the following process:

$$\begin{aligned}\hat{V} &= V_0 \quad \text{for} \quad t < t_0 \\ &= 0.75V_0 \quad \text{for} \quad t_0 < t < t_1 = \frac{\tau_{s,l}}{8} \\ &= V_0 \quad \text{for} \quad t_1 < t < t_2 = \frac{\tau_{s,h}}{4}\end{aligned}$$

$$= 0.75V_0 \quad \text{for} \quad t_2 < t < t_3 = \frac{\tau_{s,l}}{8}$$
$$= V_0 \quad \text{for} \quad t_3 < t < t\,, \tag{8.41}$$

where $\tau_{s,l}$ is the synchrotron period at the lower voltage and $\tau_{s,h}$ is the synchrotron period at the higher voltage.

b) Taking into consideration a multiparticle beam, describe the particle distribution in phase space during the process given by comparing initial and final states. Show that the the bunch length is compressed (at the expense of increased energy spread).

8.3 Harmonic Cavities

a) Verify the equations given in 8.20.

b) Sketch the relative phase between the two rf systems of Fig. 8.10 as the ratio of radiative losses to primary rf voltage varies from zero (proton beam limit) to slightly less than one.

8.4 Minimum Voltage Required for Beam Storage

The power P_γ radiated due to synchrotron radiation per turn by an electron or positron may be expressed [54] as

$$P_\gamma = \frac{cC_\gamma}{2\pi}\frac{E^4}{\rho^2}\,, \tag{8.42}$$

where c is the speed of light, $C_\gamma = 8.85 \times 10^{-5}$ m-GeV^{-3}, E is the beam energy in GeV, and ρ is the local radius of curvature of the bending magnets.

a) For an accelerator (without insertion devices) with $\rho = 2$ m and $E = 1\,\text{GeV}$, what is the total radiated power for 10^{11} particles?

b) With a 100 ns particle revolution period, at what voltage could the beam no longer be captured? What is the synchronous phase at this voltage? Assume that there are no other energy loss sources.

c) For low current beams, the electron bunch length scales with the total accelerating voltage V as $V^{-\frac{1}{2}}$. What is the disadvantage of lowering the cavity voltage for increased bunch length compared with the use of harmonic cavities?

8.5 Phase Shift along a Bunch Train

The cavity fill time τ_f describes the time evolution of the cavity voltage in response to a step function. For example, if a cavity initially at amplitude V_0 has suddenly its power source turned off, then the cavity voltage decays as

$$\hat{V}(t) = V_0 e^{-\frac{t}{\tau_f}}, \quad \text{where} \quad \tau_f = \frac{2Q}{\omega_{\text{rf}}}\,. \tag{8.43}$$

For the case of a storage ring with fast feedback, estimate the change in synchronous phase across a 500 ns long bunch train of 100 mA average beam current along the train, and cavities with a loaded Q of $Q = 3000$, a total impedance of 5 MΩ, an rf frequency of 476 MHz, and an external rf voltage of 10 MV.